micromachines

MDPI

Article

Copper-chrome-based glass heater integrated into a PMMA microfluidic system

Santiago Tovar [1], Cesar A. Hernandez [1,*] and Johann F. Osma [1]

[1] CMUA. Department of Electrical and Electronic Engineering. Universidad de los Andes, Carrera 1E # 19A-40, Bogotá, Colombia. (S.T.) s.tovar@uniandes.edu.co; (C.A.H.) ca.hernandez11@uniandes.edu.co; (J.F.O.) jf.osma43@uniandes.edu.co

* Correspondence: ca.hernandez11@uniandes.edu.co (C.A.H.)

Received: date; Accepted: date; Published: date

Abstract: The important role of a microheater in microsystems and an appropriate characterization process motivated the development of a copper-chrome-based glass heater integrated into a polymethylmethacrylate (PMMA) microfluidic system. An electrothermal analysis was carried out through a simulation and design process, to manufacture a copper-chrome layer on a transparent glass slide, fabricated through a physical vapor deposition process. Then, it was integrated with a microfluidic system made by a PMMA sheet series. The heater was characterized using the theory of electrical instrumentation, and it was compared to the simulation behavior curve and analyzed to choose a heating reference point, to control the temperature point within the fluidic system. The electrothermal results supported the simulation, as well as the chosen reference temperature point, and concluded that the system allows keeping the temperature focused, which can be used to control the temperature in different processes and to develop thermal flow sensors, with the advantage that it has the flexibility of being coupled in different systems, having optic transparency and repeatability in its process.

Keywords: microheater; microsystem; electrothermal systems, thermal characterization, hysteresis, PVD, PMMA.

1. Introduction

Heating in microsystems, referred to as microheaters, has a fundamental role in different microsensors, as thermal flow sensors [1]; in embedded systems [2,3], as the operating temperature to control environments for chemical and biological processes at small scales [4]; and inclusive for thermal electric generation on microchannels [5]. The temperature control of microsystem devices can also be achieved using macroscale equipment, such as incubators and surface heaters. This type of equipment usually consumes a considerable amount of electricity and does not allow to perform parallel, system-specific adjustments. Moreover, these macroscopic temperature controls, even if precise, have slow time responses [6].

The design of temperature controls directly integrated into the microsystem architecture [7] is an auspicious alternative that has been credited for the development of polymerase chain reaction integrated microsystems [8], protein characterization and sensing [9], and supported bilayer lipid membrane-based biosensors [10], among others. These microsystems employ a thin film of deposited metal as an electrically resistive heating element, as described by Joule's law. The importance of having a direct contact between the heater and the system relies in having control and certainty about the conditions of the elements immersed in the microsystem, due to a resistance reduction to the heating transference [11]. Additionally, having the possibility to include thermal sensors as films within the system [12].

A good characterization process on a heating system gives better results in the operating temperature [13,14]. For instance, the work published by Scorzoni highlights the advantages of

implementing electrothermal simulations to compare and analyze the characterization process on a heating system, as well as for defining the optimal geometric design for the concentric microstructures where rectangular trenches provide a better heat concentration and then fewer heat losses [14].

In this paper, a copper-chrome-based glass heater integrated into a PMMA microfluidic system was developed, together with an electrothermal design and simulation process. The manufacturing method consists of physical vapor deposition of a copper-chrome layer on a transparent glass slide, and the integration with a microfluidic system. This microfluidic system was fabricated with a PMMA sheet series, glued with transparent double-sided tape and methylene chloride. A leak test was performed, and the heater was characterized, which was compared to the simulation characterization and analysed to choose a heating reference point. From the reference heating, a control current system was designed and implemented to keep the temperature point within the microfluidic system.

2. Materials and Methods

2.1 Materials, Equipment and Software

Polymethylmethacrylate (PMMA) sheets with a thickness of 2 mm and 3 mm were bought from Diacrílicos J.D. (Colombia). Glass slides with dimensions of 25.4 mm x 7.2 mm x 1.2 mm, purchased from vendor Sail Brand (Yancheng, China). Chrome pieces, Cr, purity of 99.95%, with a size range between 0.8 mm to 6 mm, and copper pellets, purity 99.99%, with a diameter of 6.35 mm and a length of 6.35 mm were acquired in Kurt J. Lesker Company (Clairton, PA, USA). Analytical grade methylene chloride was used.

Physical vapor deposition (PVD) process was performed using thermal evaporator Edwards E306 (Moorfield Nanotechnology Limited, Knutsford, Cheshire, UK) and in a cleanroom facility environment. Likewise, spin coating processes were performed using SPIN150 spin coater (SPS Europe B.V., Putten, The Netherlands). UV pattern exposure was performed using a Karl-Suss MJB-3 Aligner (SÜSS MicroTec SE, Garching, Germany), positive photoresist MICROPOSIT™ SC™ 1827 (SC-1827) and developer MICROPOSIT™ MF™ 319 (MF-319 developer) were purchased from Rohm and Haas Electronic Materials LLC (Marlborough, MA, USA). Baker PRS-1000 stripper (stripper) for lift-off processes was purchased from Avantor (Radnor, PA, USA).

The prototypes of the PMMA slides were fabricated with a laser cutting machine Trotec® SPEED 100 (Trotec Laser GmbH, Marchtrenk, Austria). Transparent double-sided tape TESA, with a thickness of 12 mm (Tesa SE, Hamburg, Germany), was used for sealing of the microdevices. Special glue for model-building, handicraft, and repair UHU HART, was used for gluing of coupling connectors (UHU GmbH & Co. KG, Bühl, Germany).

The design of the printed circuit board (PCB) was elaborated using EAGLE 8.3.2 PCB Design Software (Autodesk, San Rafael, CA, USA). The design of the PMMA microsystems was developed using AutoCAD 2020 Design Software (Autodesk, San Rafael, CA, USA). A thermoelectric analysis simulation was implemented in COMSOL Multiphysics 5.3 (COMSOL, Inc., Burlington, MA, USA).

Supply and measurements for the microsystem characterization process were carried out with variable dual voltage source HAMEG ™ HM7042 (HAMEG Instruments GmbH, Mainhausen, Germany), digital multimeter PeakTech Multifunction Tester® 3725 (PeakTech Prüf- und Messtechnik GmbH, Ahrensburg, Germany), infrared thermometer UNI-T® UT302B (UNI-TREND technology CO., LTD., Dongguan, China) and thermal camera Panasonic AMG8833 (Panasonic Industrial Devices Company, Newark, NJ, USA).

The simulation of the temperature control system with the current source (IC) was developed in LTSpiceXVII of Analog Devices (Analog Devices, Inc. (ADI), MA, USA), and this IC was compounded with 2N2222 transistors from Microsemi (Microchip Technology Inc, AZ, USA), a 15 Ω metal film resistor 0.5 W 1% (KOA Speer Electronics Inc., Bradford, PA, USA) and an adjustable trimmer 100 Ω BOURNS 3296 W-1-101_LF (Bourns Inc., Riverside, CA, USA).

The measurements of the microsystem heater were performed with thermographic camera Keysight U5855A JP54270688 (Keysight Technologies, Santa Rosa, CA, USA) and syringe infusion pump Medcaptain MP-30 (Medcaptain Medical Technology Co. Ltd., Guangdong Sheng, China). To perform the leak test and report the thermographic camera results, transparent water-based olive green (956) dye made with pigments and with a matte finish ROSETA (ROSETA INDUSTRIAL LTDA, Colombia) was used.

2.2. Copper and Chrome Deposition

For the substrate fabrication of the copper-chrome-based glass heater (Heater), first, it was deposited a 15 nm chrome nanolayer, a physical thermal deposition, for a 10 mg chrome evaporation, was achieved using a tungsten heating filament. A vacuum pressure of 7×10^{-6} mbar and an evaporation rate of 1 nm/s were established. After, a 250 mg copper evaporation was performed with the same evaporation parameters. As a result, it was obtained films with a 115 nm thickness compounded by a 15 nm chrome nanolayer and a 100 nm copper nanolayer.

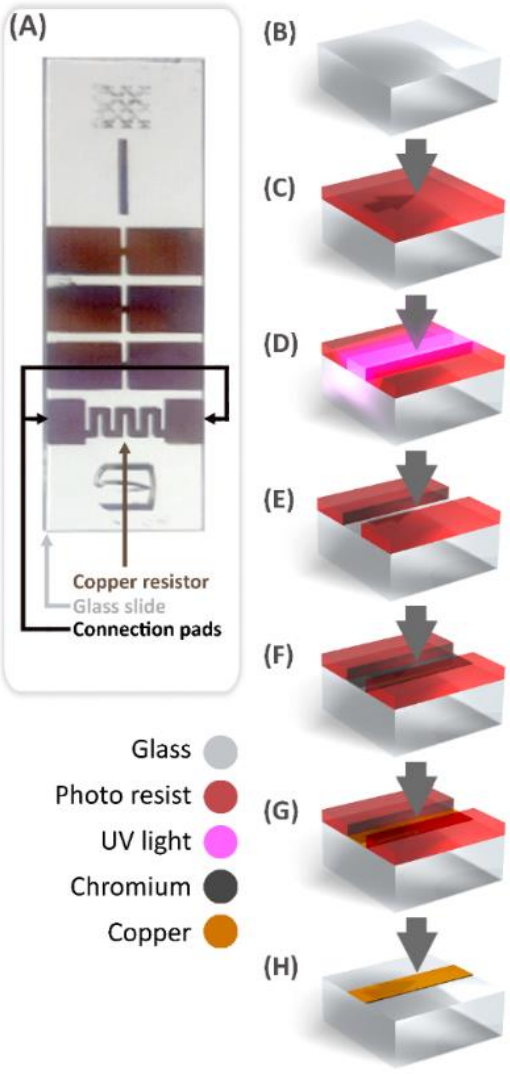

Figure 1. Fabrication process of the copper-chrome-based glass heater (**A**) Photograph; (**B**) Clean glass surface; (**C**) Photoresist covered glass; (**D**) UV light exposure; (**E**) Photoresist development; (**F**) Chrome deposition; (**G**) Copper deposition (H) Final heater structure on glass after stripping off photoresist.

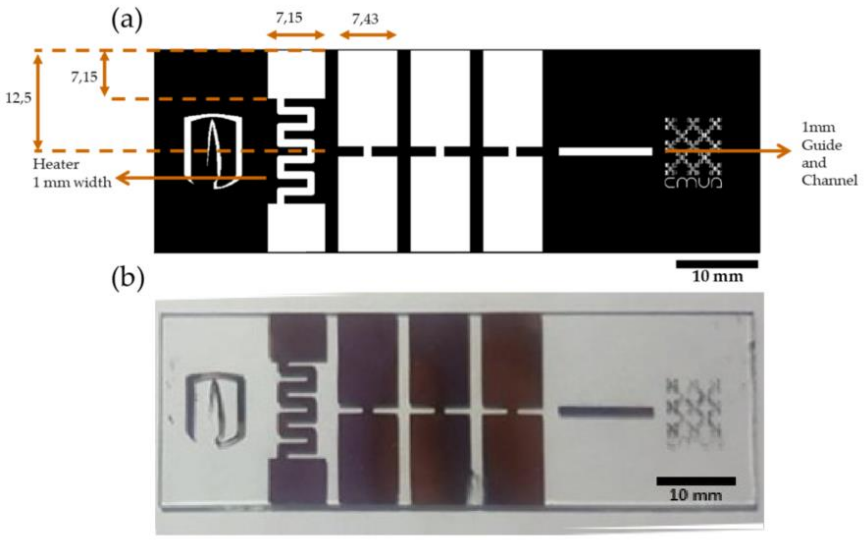

Figure 2. (**a**) Final design mask with dimensions; (**b**) Copper-chrome-based glass heater after PVD process

Table 1 shows the common theoretical calculations for the resistance of the copper-chrome-based heater, where the heater resultant resistance is the sum of both the pads and heater resistance, which are the parallel configuration between the copper and the chrome resistance. As a result, the theoretical resistance of the heater was 4.80 Ω.

Table 1. Measurements and common theoretical calculations of the copper-chrome-based heater

Item	Copper	Chrome	Heater
Height (nm)	100	15	115
Resistivity (Ω·mm²/m) [15]	0.017	0.125	-
Pads area (mm²)	0.00125	0.0001875	-
Pads length (mm)	7.43	7.43	-
Heater length (mm)	31	31	-
Paths resistance (Ω)	0.101	4.9538	0.0989
Heater resistance (Ω)	5.301	38.75	4.66
Heater resultant resistance (Ω)	5.402	43.73	4.80

Then, practical heater resultant resistance was measured, with four samples for five identical heaters, produced as explained in the deposition process, with a mean result of 9.11 Ω and variance of 0.17 Ω. Additionally, the microsystem coupling wire resistance was measured, with a mean value of 1.4 Ω and a variance of 0.22 Ω.

The common theoretical resistance calculated is less than the practical resistance measured with respect to the heater, owing to the effects of resistivity on thin films that must be considered with a different model.

An appropriate model can be used for materials that are reduced to dimensions on the nanoscale, in which many of the common properties or characteristics are no longer valid, and, likewise, it has been shown that the mechanical, thermodynamic, electrical, and optical properties are altered due to size difference. The reasons for this change in properties are related to increased surface interactions, as well as absorption and dispersion effects [16].

The model allowed to conclude that the electrical resistivity of a thin film on nanometric scales increases exponentially as the thickness of that film decreases in size [16]. Therefore, the theoretical resistance is closer to the resistance measured in the heater.

2.3. Microsystem Fabrication

2.3.1 Acrylic Plates Fabrication

In Figure 3, on the left side, it is depicted the final layered plate design of the PMMA microsystem. As it is observed, the engraving of 1 mm is indicated in green (Figure 3b.) at the microchannel plate (Figure 3a), it played a fundamental role when is coupled with the heater adjustment plate (Figure 3d), which is dimensionally adjusted to the heater. The spaces seen in the microchannel plate corresponded to the coupling pads used for wiring (Figure 3c), where the current source for the designed heater resistor is supplied. The support plate (Figure 3e) was used in the prototype base with a second glass slide to give it the same thickness to the area for the glass placement.

At the right side of Figure 3 is the cutting plane of black acrylic plates used to isolate the system from light, where the thermographic camera adjustment plate (Figure 3f) was the layer implemented for the characterization with the thermographic camera, which was used for the final results report with water flow inside the microsystem, and the characterization plate for thermal camera (lens) (Figure 3g) and the characterization plate for thermal camera (body) (Figure 3h) were used for the characterization with the thermal camera.

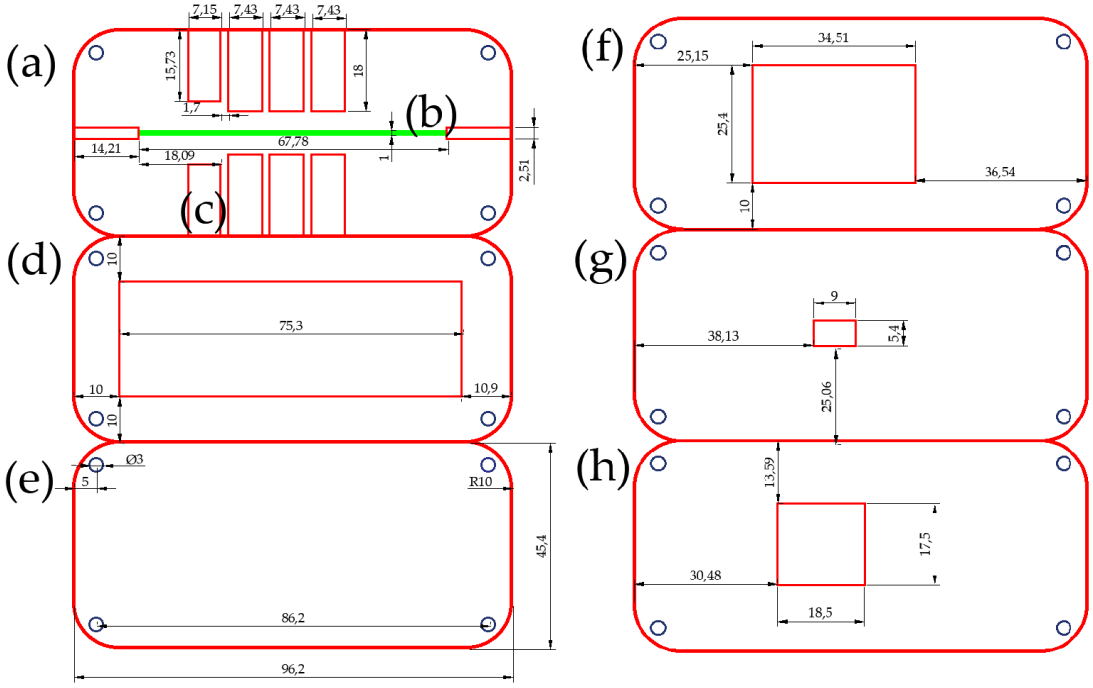

Figure 3. Cut layouts of the microsystem PMMA plates (the reference screw holes are highlighted in blue color): (**a**) Microchannel plate; (**b**) Microchannel (highlighted in green); (**c**) its coupling pads; (**d**) Heater adjustment plate; (**e**) Support plate; (**f**) Thermographic camera adjustment plate; (**g**) Characterization plate for thermal camera (lens); (**g**) Characterization plate for thermal camera (body).

The technique for the microsystem fabrication was developed at the CMUA Research group at Universidad de Los Andes. This technique consists of a series of previously characterized 1 mm cuttings and engravings with a laser-cutting machine on a layer of PMMA [17]. The engravings were used to build and support the structure for microsystem water flow and the heater. To assemble the acrylic plates and the heater, a double-side tape was used, which was previously cut by using the laser-cutting machine.

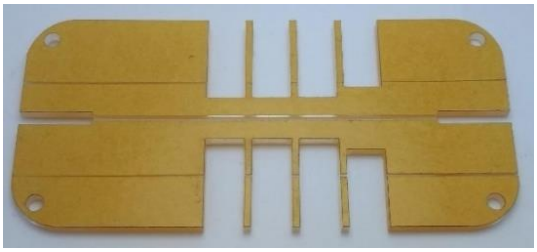

Figure 4. Platelayer where the microchannel is engraved on the double-sided tape.

2.3.2 Microsystem Bonding Process, Final Assembly and Leak Test

After the acrylic plates and the heater were fabricated, both were cleaned with alcohol for the gluing process. This process began coupling both, the heater and an extra glass slide to the heater adjustment plate (Figure 3d), then, the protection of the adhesive was removed from the platelayer, displayed in Figure 4, and both layers were aligned using the reference screw holes, and the reference line of the heater micro conduct, both referenced in Figure 3. Notably, the layer with the micro conduct was in contact with the heater as it gave more precision to the temperature control of the heated fluid, both platelayers were glued with the double-sided tape.

The support plate (Figure 3e) and the back layer of the heater adjustment plate (Figure 3d) were glued. This process was performed by dispersing methyl methacrylate solution (MMA) between the acrylic platelayers to be glued, in this step the same references as used in the previous process for an appropriate alignment. Later, this coupling was forced to hold a 5 Kg weight during a drying time of 18 hours. After this drying time, the coupling connectors to the microsystem were added with the adhesive for modeling (HART), then, the microsystem was again exposed to drying time. Coupling connectors were glued to perform the connection with a catheter, which drove the flow from the syringe infusion pump.

For the first characterization step, the characterization plate for the thermal camera (lens) and characterization plate for the thermal camera (body) (Figure 3g and Figure 3h respectively) were glued to the top layer of the microchannel plate (Figure 3a), wherein another layer was the microchannel coupled with the heater. Meanwhile, for the result probes, the thermographic camera adjustment plate (Figure 3f) were glued to the top layer of the microchannel plate, for giving the test measurements a wider visual angle.

In Figure 5, the final assembly of the microsystem is shown, using the two characterization plates (lens and body) for thermal camera (Figure 3g and Figure 3h) and using the thermographic camera adjustment plate (Figure 3f) for the test measurements of the microsystem. It can be noted that the light transmission is avoided in the structure outside of the window area, to carry out the correct data and photo recording with both cameras.

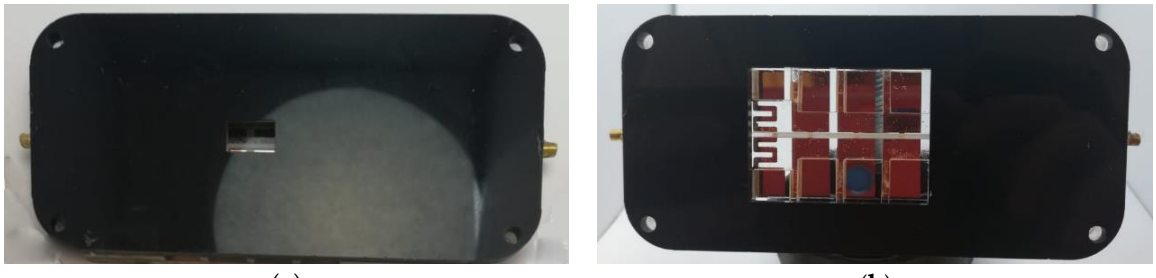

(**a**) (**b**)

Figure 5. Total mounting of the microsystem, from the face where it fully shows all the components of the system: (**a**) Characterization mounting; (**b**) Test measurements mounting.

Finally, to determine leaks and performance of the applied microflow, the complete microsystem was evaluated using a vacuum test with two empty syringes connected in both microsystem coupling connectors, and a series pressure configuration of 12 ml/h with the syringe infusion pump, where air

was used first as fluid, and then, water with transparent water-based green dye (concentration of ~ 3%), to observe the flow transition within the system.

2.3.3 Heater Circuit Design Process and Electrothermal Simulations

To have better control of the temperature measured at the heating point of the microsystem, a reference point of the characterization obtained in the results was taken. Specifically, an applied voltage of 2.47 V was chosen, corresponding to a temperature range of 70 ± 3 °C. Additionally, a current of approximately 280 mA was measured. Then, thermoelectric simulations were used to compare and predict the thermal behavior of the heater according to the voltage point sourced, so this simulation was developed and designed with similar properties and the same dimensions of the fabricated heater and its heating point, as shown in Table 2.

Table 2. Properties used in the electrothermal simulation in Comsol Multiphysics ™, where most of the properties given by the material selected in the simulation.

Item	Value
Initial water temperature (°C)	20
Initial air temperature (°C)	20
Copper electrical conductivity (S/m)	5.96 * 10 ^{7}
Chrome electrical conductivity (S/m)	7.9 * 10 ^{7}
Water heat transfer film coefficient (W/(m^2*K)) [18]	300
Air heat transfer film coefficient (W/(m^2*K)) [19]	20.45
Copper layer thickness (nm)	100
Chrome layer thickness (nm)	15

Therefore, simulations consider the electrical and thermal characteristics of the glass substrate and the chrome-copper resistor of the heater. As a result, it was obtained a concentrated thermal distribution simulation, exposed in Figure 6, with a similar heat reference point at the chosen voltage, showed in Figure 7, then it was concluded that this range would be aimed in the heating control circuit.

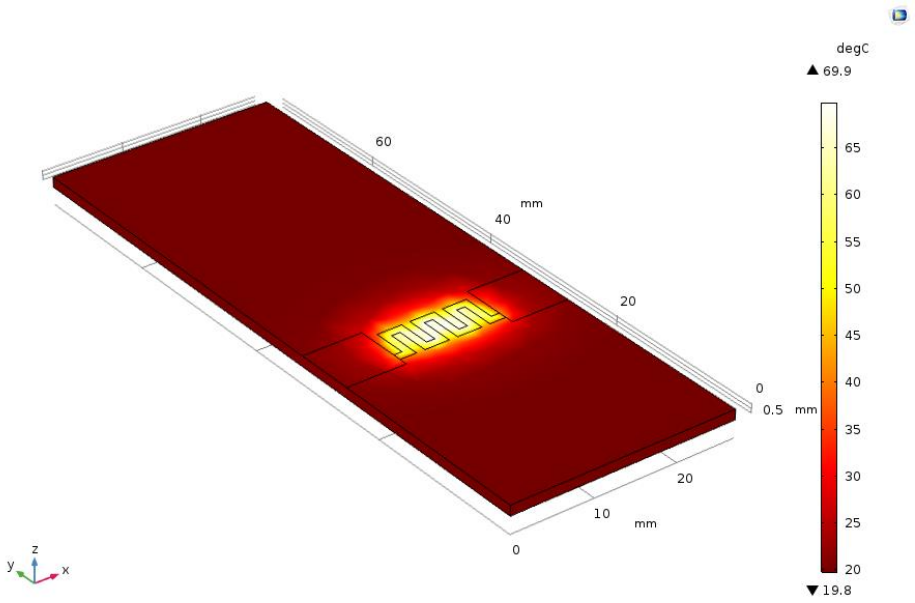

Figure 6. Thermal distribution simulation (°C), where it is immersed in water and air at room temperature, with the same heater sizes and similar properties as the heater, shown in Table 2.

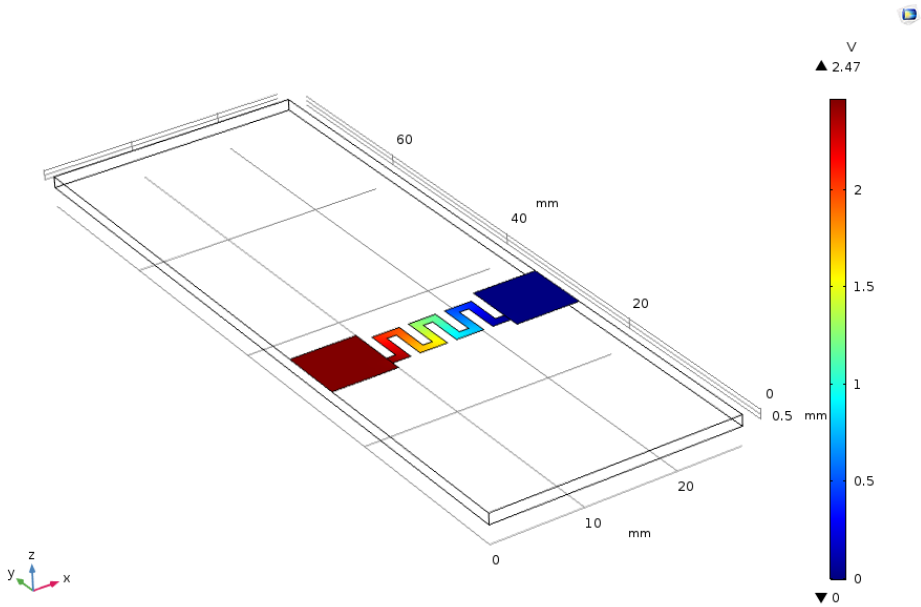

Figure 7. Simulation of the electrical distribution (V), with the same heater sizes and similar properties as the heater, shown in Table 2.

The peak temperature in the thermal distribution simulation was 69.8 °C, as given by the voltage reference point. Additionally, a heating behavior simulation characterization curve was made, as is shown in Figure 8, where is marked this heating control point.

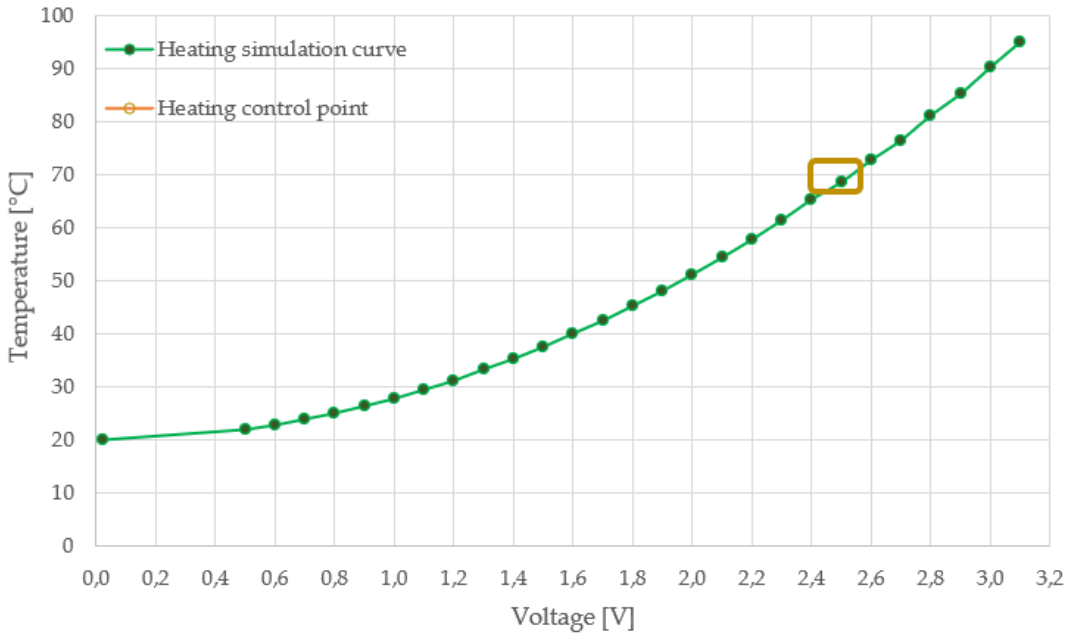

Figure 8. Simulation heating behavior characterization curve based in 0.1 V step changes.

This simulation worked according to the Figure 9a with an output of 2.47 V in the heater resistance and a current of 270.5 mA, which is at the beginning of the chosen work area, also, as an indicator of good source performance [14,20], it was found to have an increase of 0.1 V and 10 mA by the temperature increase in the circuit, so it was at the precise point of operation.

Consequently, a current source was designed to set the current used in the heating system. The temperature control system design and its simulation were developed implementing 2N2222 transistors, to obtain a collector current of 300 mA, and, although there are mirrors or commercial

encapsulated current sources, which are much more stable in their behavior, they did not get to provide this current intensity.

The calculated current source was then implemented in a PCB, as is observed in Figure 6b, in which the current was fixed by a reference resistance with a higher value than in the simulation, and that, in a parallel configuration with a trimmer, would make possible to lower the resistance to any specified value, and adjusting the resistance value, if necessary, to change the reference resistance to the point at which the system would be worked.

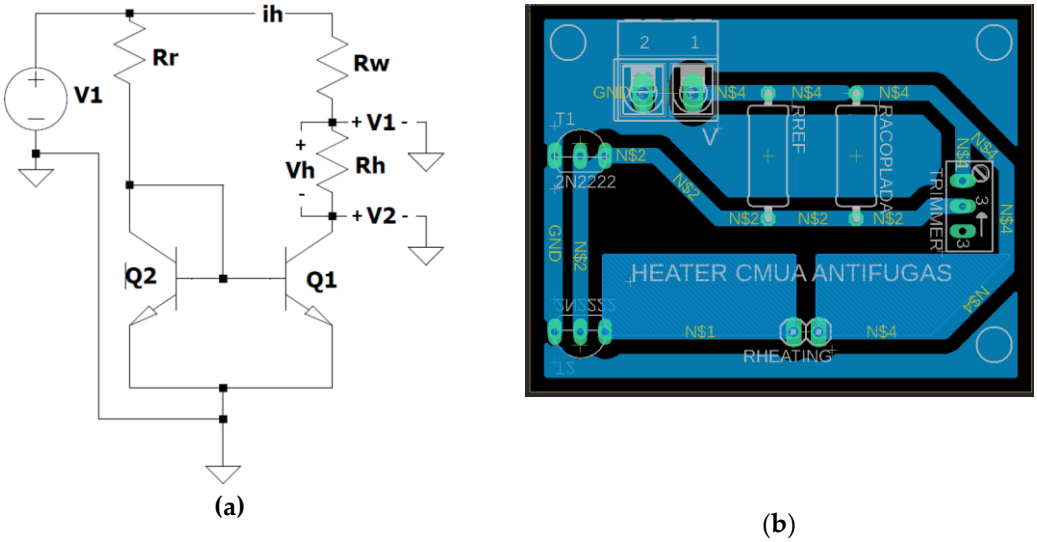

Figure 9. Heater circuit design: (**a**) Simulation within reference point, where: V1 (source Voltage circuit) = 5 V, Rr (Reference resistance) = 15 Ω , Rw (coupling wire Resistance) = 1.4 Ω, Rh (homologated Resistance heater) = 9.11 Ω, Q1 and Q2 (current mirror 2N2222 transistors), ih (current circuit) = 270,55 mA, V1 (Voltage between homologated resistance heater and ground) = 4.62 V, V2 (collector-emitter Q1 Voltage) = 2.16 V, Vh (resistance heater Voltage, V2-V1) = 2.47 V; (**b**) PCB Design with the reference resistance and the 100 Ω parallel adjustment trimmer.

Lastly, power consumption simulation was implemented through a comparison between the temperature vs voltage simulation and the given resistance from the characterization. This is shown below in Figure 10.

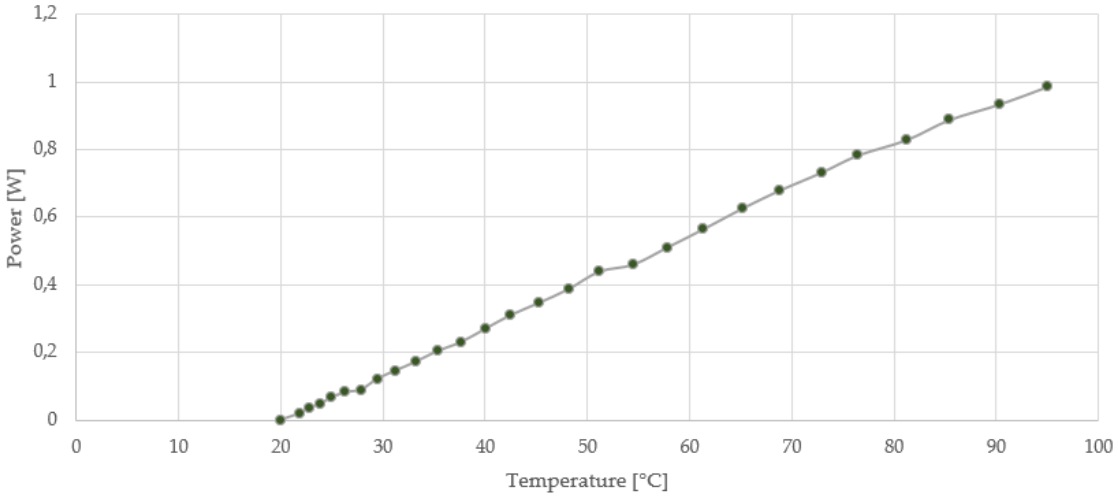

Figure 10. Simulation power consumption based in resistance characterization curve.

3. Results

3.1. System Characterization

The characterization and calibration curves were developed to include the system hysteresis, this must be defined by a heating curve (up) and a cooling curve (down). A hysteresis curve, given by the theory of electrical instrumentation [21], is obtained by the following equation:

$$(H=|Y_1-Y_2|). \quad (1)$$

Where Y_1 is the resulting response of the heating curve and Y_2 of the cooling curve. These characterization curves were elaborated using both the thermal camera and the infrared thermometer, with four samples, in steps of 0.1 V by voltage variation.

For the characterization with the thermal camera, the determined time of stabilization to measure the step was 10 seconds. Figure 117 shows the pictures captured during the calibration by the thermal camera, the concentrated distribution of heat within the heater zone can be observed.

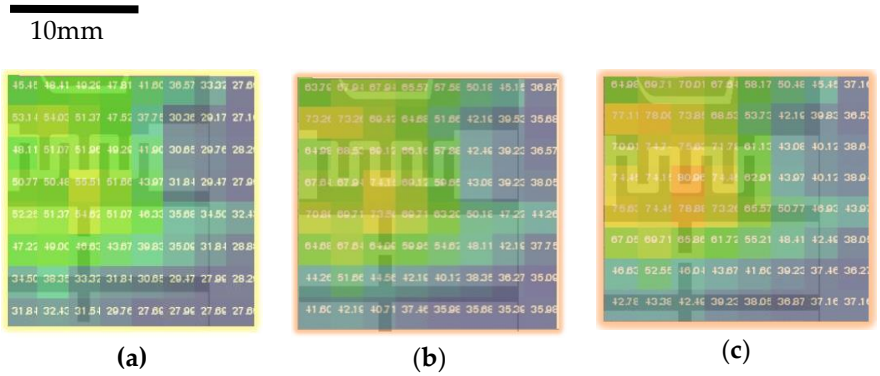

Figure 11. Captures of the thermal camera with: (**a**) Voltage of 2 V (peak temperature of 55°C); (**b**) Voltage of 2.5 V (peak temperature of 75°C); (**b**) Voltage of 3 V (peak temperature of 82°C).

The characterization with the infrared thermometer was performed using the center of the heater as a focal point, with the same determined time of stabilization to measure (10 seconds). The calibration curves, for the heating system, are depicted in Figure 12.

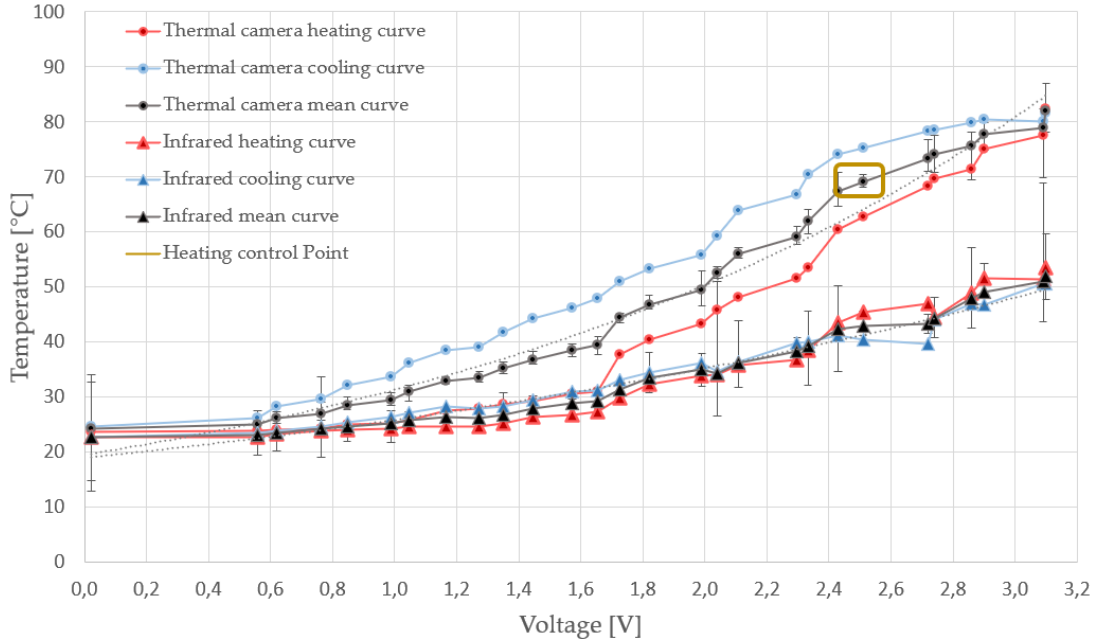

Figure 12. System characterization for the thermal camera and infrared system based in 0.1 V step changes.

In the last Figure, it can be observed that the measurements of the calibration curve acquired by the thermal camera are lower than the ones obtained by the infrared thermometer. Then, the characterization using the thermal camera can be considered more accurate than the curve of the infrared thermometer, due that the thermal camera has better accuracy in its heat point focus, and that its measurements are not affected by light reflection in the glass. Starting with this premise, power consumption was measured with an infrared thermometer calibration curve, as shown in Figure 13.

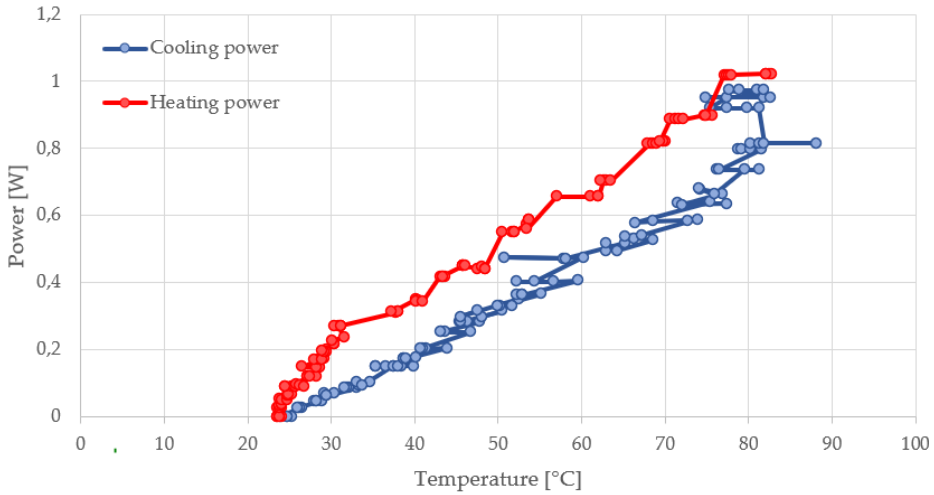

Figure 13. Power consumption vs temperature curve.

3.2. Heating Control Circuit

For the evaluation of the current source, it was observed, during the first voltage and current tests, a current value of 280 mA and a voltage value of 2.49 V, where the resistance of the heater was homologated with a fixed resistance, also including the resistance of the cables and the pads that surround the heater rectangular serpentine shape at the time of stabilization. Then, the printed circuit board for this current source was assembled, where a voltage of 2.52 V and a current of 283 mA were acquired at its output by simulating the same heating resistance with the homologated resistance value. Finally, the measurements were 2.53 V in its output voltage and 279 mA of current with the heater and its coupling wires.

3.3. Thermographic Camera Results and Final Assembly

The final assembly is shown in Figure 14, where the microsystem was connected by the coupling wires with the heating control system, and a syringe infusion pump, with a flow rate of 12 ml/h. The microsystem was connected via catheter, as mentioned in the materials and methods section. The fluid immersed in the system is the same as the leak test, hence water with transparent water-based green dye (concentration of ~ 3%), to observe the flow transition within the system.

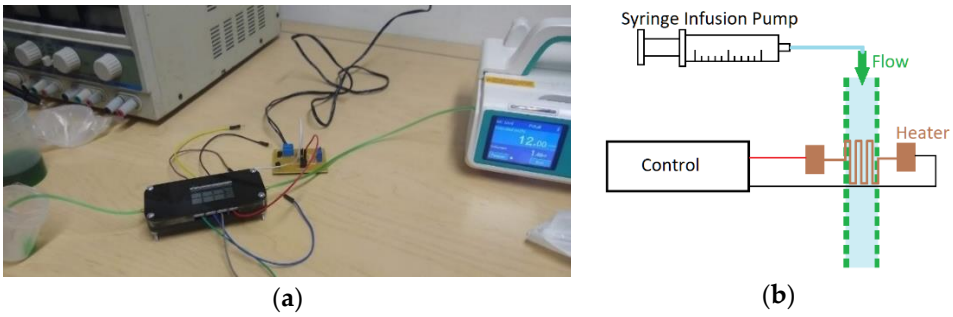

Figure 14. Final assembly to final test with a thermographic camera: **a)** Photograph; **b)** Schematic representation of the final assembly.

Shown below are the obtained results with the thermographic camera in different samples at the microsystem, coupled with the current control circuit. the reference temperature was 21.3 °C during the measurements, and the temperature obtained at the stabilization time was around 71.3 °C, as it is observed in Figure 15.

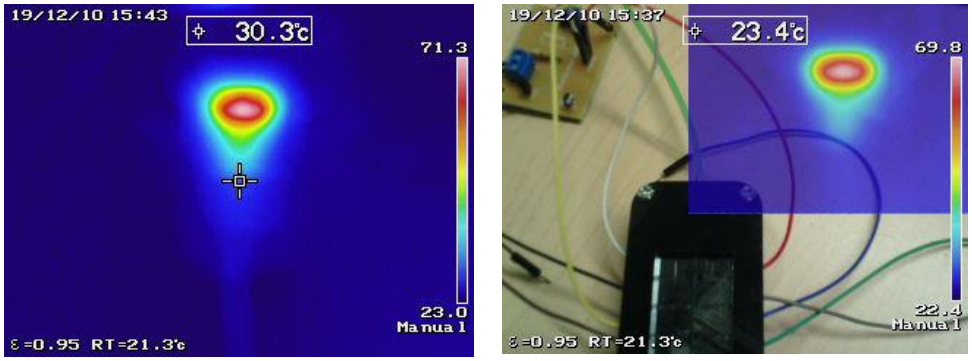

(**a**) (**b**)

Figure 15. Thermographic camera results in its captures with a controlled flow of 12 ml/h: **a**) Full-screen capture; **b**) Capture in a combined photo that shows the microsystem focalized.

Testing with different flows was performed to inspect the heat velocity phenomenon, shown in Figure 16. The maximum temperature observed at the focal point was near 115 °C, this temperature was generated with the same applied current, which was maintained stable with the current control circuit, however, the overall power in the heater was increased, this might be related to the effect of the resistance diminution caused by the flow of water. It is shown how the rate of temperature distribution was expanded as the syringe pump was given an increased velocity of the fluid within the microsystem. These tests results allow to conclude that the system allows keeping the temperature focused, which can be used to control the temperature in different processes and to develop thermal flow sensors.

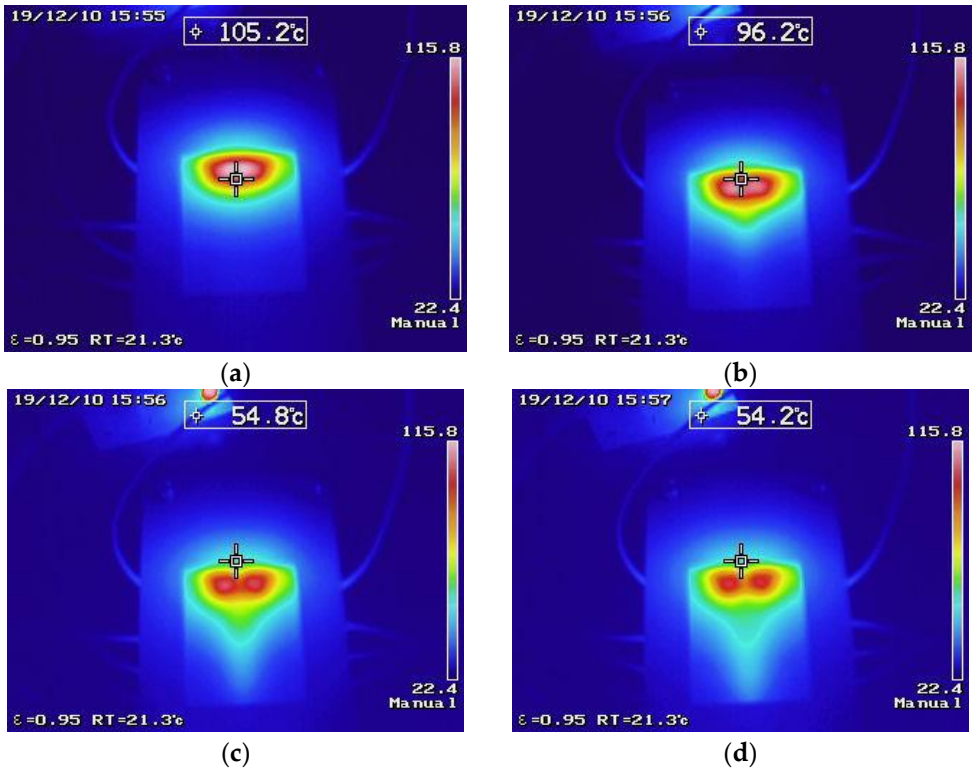

(**a**) (**b**)

(**c**) (**d**)

Figure 16 Thermographic camera results in testing with different flows to inspect the heat velocity phenomena: (**a**) 5 ml/h; (**b**) 10 ml/h; (**c**) 15 ml/h; (**d**) 20 ml/h.

4. Discussion

The presented results support the electrothermal simulation, as well as the chosen point reference temperature, as is showed in Figure 17, also the system keeps the heat point of concentration and incorporates a more robust temperature control for microenvironments. Likewise, the measurements obtained about power consumption have an adjusted behavior from the consumption simulation, just like is represented in Figure 18. These results have an approximate of 7,22% and 5,42 % error, respectively. Furthermore, the thermographic camera results shows how there was a temperature velocity change as the flow increased, supplied with the syringe pump, these changes can be used to determinate microflows, by the incorporation of thermal sensors, which can be fabricated using techniques analog to the ones used in this work, to develop thermal flow sensors for microsystems. This heater has the flexibility of being coupled in different systems, with the uses afore mentioned, with the advantage of having optical transparency and repeatability in its process, specifically in the vapor deposition process.

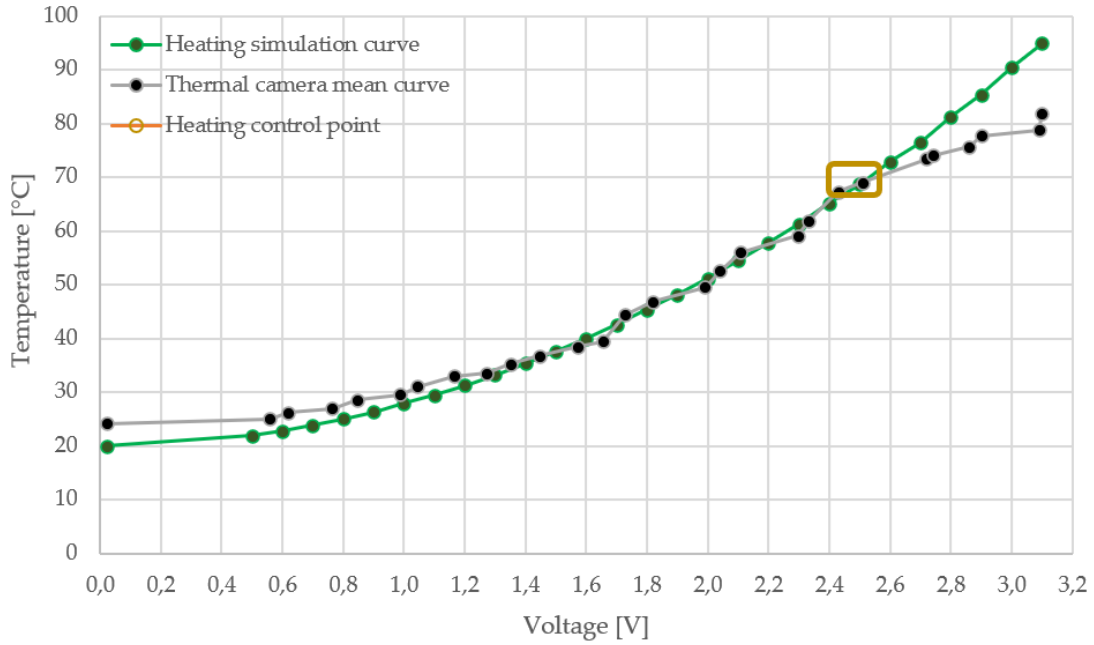

Figure 17. Comparison system characterization between thermal camera mean curve and heating behavior simulation characterization curve based in 0.1 V step changes.

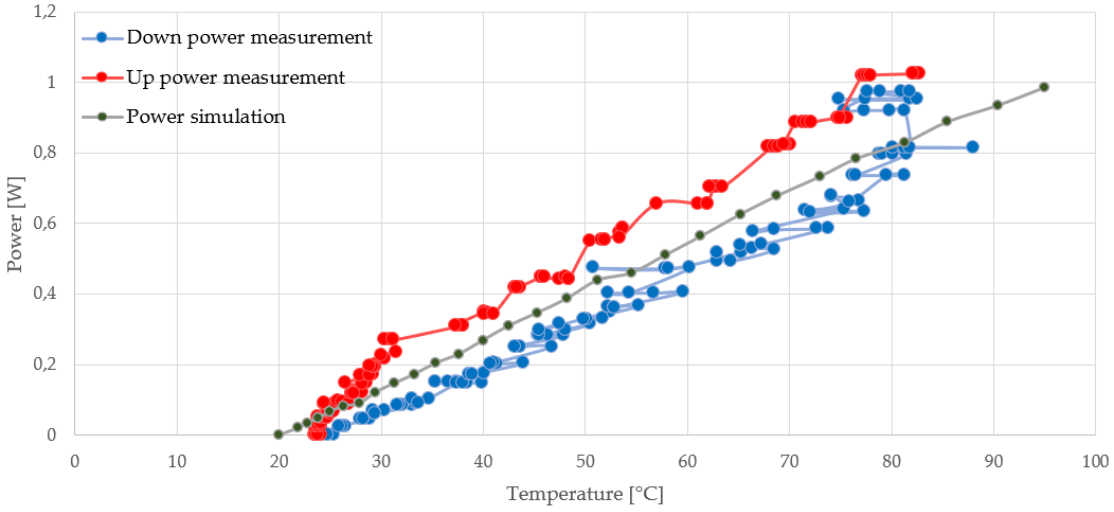

Figure 18. Comparison power consumption between thermal camera results and simulation curve.

Otherwise, the comparison in Figure 17 shows within the range between 2.6 V and 3.2 V a difference of temperature output response, which could be explained due to the ideal conditions of the simulation. Then, in future investigations, this characterization process could have more than 10 seconds to give better results of response. Besides, the fabricated microsystem development has a lot of possible applications, like fabricated different coupling systems, that it might have less thermal convection loss within the lab-on-chip, with an analysis of the contact resistance between the pads and the cables of the sensors. And so, the voltage output at said temperature response might have better behavior. At last, using another material as Platinum in the prospective characterization process for microheater, may decrease response time and allow a more linear characterization curve, to use a wider temperature range.

Author Contributions: For research articles with several authors, a short paragraph specifying their individual contributions must be provided. The following statements should be used "Conceptualization, X.X. and Y.Y.; methodology, X.X.; software, X.X.; validation, X.X., Y.Y. and Z.Z.; formal analysis, X.X.; investigation, X.X.; resources, X.X.; data curation, X.X.; writing—original draft preparation, X.X.; writing—review and editing, X.X.; visualization, X.X.; supervision, X.X.; project administration, X.X.; funding acquisition, Y.Y. All authors have read and agreed to the published version of the manuscript.", please turn to the CRediT taxonomy for the term explanation. Authorship must be limited to those who have contributed substantially to the work reported

Funding: The work of CAH was founded by the Colombian Ministry of Education and the Administrative Department of Science, Technology and Innovation, Colciencias, through the program for national doctorates, grant 567.

Acknowledgments: The authors want to acknowledge the technical contribution to the cleanroom of the Department of Electrical and Electronics Engineering, specially to Alfredo Sanchez, in the heater fabrication process; as well as to Juliana Noriega, Paula Peñaranda, Ana Lucia Campaña, Diana Sotelo, Andres Aranguren, Master's students at the Electrical and Electronic Engineering Department, in the support in the microsystem fabrication process; and to Brayan Ariza, ungraduated's student at the Electronic Engineering Department, in the characterization and calibration curves with the thermal camera. This work was supported by the CMUA group of the Universidad de los Andes.

Conflicts of Interest: The authors declare no conflict of interest.

References

1. Khan, B.; Ahmed, S.; Kakkar, V. A Comparative Analysis of Thermal Flow Sensing in Biomedical Applications. *Int. J. Biomed. Eng. Sci.* **2016**, *3*, 01–07.
2. Keshavaditya, G.; Eranna, G.R.; Eranna, G. PRT embedded microheaters for optimum temperature distribution of air-suspended structures for gas sensor applications. *IEEE Sens. J.* **2015**, *15*, 4137–4140.
3. Hayakawa, T.; Sakuma, S.; Fukuhara, T.; Yokoyama, Y.; Arai, F. A Single Cell Extraction Chip Using Vibration-Induced Whirling Flow and a Thermo-Responsive Gel Pattern. *Micromachines* **2014**, *5*, 681–696.
4. Hernandez, C.A.; Osma, J.F. Microbial Electrochemical Systems: Deriving Future Trends From Historical Perspectives and Characterization Strategies. In *Frontiers in Environmental Science*; 2020; Vol. 8, pp. 1–19.
5. Rezania, A.; Rosendahl, L.A. Thermal effect of a thermoelectric generator on parallel microchannel heat sink. *Energy* **2012**, *37*, 220–227.
6. Velve-Casquillas, G.; Le Berre, M.; Piel, M.; Tran, P.T. Microfluidic tools for cell biological research. *Nano Today* **2010**, *5*, 28–47.
7. Jiang, L.; Wong, M.; Zohar, Y. Unsteady characteristics of a thermal microsystem. *Sensors Actuators, A Phys.* **2000**, *82*, 108–113.
8. Lagally ET; CA, E.; RA, M. Fully integrated PCR-capillary electrophoresis microsystem for DNA analysis. *Lab Chip* **2001**, *1(2)*, 102–107.

9. Liu, X.; Li, L.; Mason, A.J. Thermal control microsystem for protein characterization and sensing. *2009 IEEE Biomed. Circuits Syst. Conf. BioCAS 2009* **2009**, 277–280.
10. Tvarogek, V.; Tienb, H.T.; Novotny, I. Thin-film microsystem applicable in (bio) chemical sensors. *Sensors Actuators, B Chem.* **1994**, *19*, 597–602.
11. Wojtas, N.; Hierold, C. Microfluidic heat transfer systems optimized for thermoelectric heat exchangers. *2013 Transducers Eurosensors XXVII 17th Int. Conf. Solid-State Sensors, Actuators Microsystems, TRANSDUCERS EUROSENSORS 2013* **2013**, 1368–1371.
12. Pawlak, R.; Lebioda, M. Electrical and thermal properties of heater-sensor microsystems patterned in TCO films for wide-range temperature applications from 15 K to 350 K. *Sensors (Switzerland)* **2018**, *18*.
13. Je, J.; Lee, J. Design , Fabrication , and Characterization of Liquid Metal Microheaters. *Microelectromechanical Syst.* **2014**, *23*, 1156–1163.
14. Scorzoni, A.; Caputo, D.; Petrucci, G.; Placidi, P.; Zampolli, S.; de Cesare, G.; Tavernelli, M.; Nascetti, A. Design and experimental characterization of thin film heaters on glass substrate for Lab-on-Chip applications. *Sensors Actuators A Phys.* **2015**, *229*, 203–210.
15. Serway, R.A.; Jewett Jr, J.W. *Physics for Scientists and Engineers with Modern Physics*; 9th ed.; Brooks/Cole: Boston, MA 02210, 2014; ISBN 9781133954057.
16. Lacy, F. Developing a theoretical relationship between electrical resistivity, temperature, and film thickness for conductors. *Nanoscale Res. Lett.* **2011**, *6*, 1–14.
17. Campaña, A.L.; Sotelo, D.C.; Oliva, H.A.; Aranguren, A.; Ornelas-Soto, N.; Cruz, J.C.; Osma, J.F. Fabrication and characterization of a low-cost microfluidic system for the manufacture of alginate-lacasse microcapsules. *Polymers (Basel).* **2020**, *12*.
18. Solidworks SOLIDWORKS Web Help.
19. Khabari, A.; Zenouzi, M.; Connor, T.O.; Rodas, A. Natural and Forced Convective Heat Transfer Analysis of Nanostructured Surface. *Proc. World Congr. Eng.* **2014**, *I*, 7–9.
20. Cadar, S. Simulation & Modelling of a Tungsten Filament with COMSOL for Electrothermal Process. *IEEE 22nd Int. Symp. Des. Technol. Electron. Packag.* **2016**, 165–170.
21. Perez, M.A. Instrumentación electrónica. In; Paraninfo, E., Ed.; 2014; pp. 7–12 ISBN 8428337020.